therefore to be necessary.

Acknowledgment. We thank the Deutsche Forschungsgemeinschaft, the Stiftung Volkswagenwerk, and the Fonds der Chemischen Industrie for financial support.

Registry No. $[Fe(2\text{-pic})_3]Br_2 \cdot EtOH$, 71521-13-6.

Supplementary Material Available: Listings of structure factor amplitudes, anisotropic temperature factors, calculated hydrogen positions of the ethanol molecule, and least-squares planes of the pyridine rings (27 pages). Ordering information is given on any current masthead page.

Contribution from the Institute of Inorganic Chemistry, University of Münster, D-4400 Münster, Federal Republic of Germany, and Chemistry Department A, Technical University of Denmark, DK-2800 Lyngby, Denmark

Crystal Structure and Infrared and Raman Spectra of $KV(SO_4)_2$

Rasmus Fehrmann,*[1a] Bernt Krebs,[1b] G. N. Papatheodorou,[1c,d] Rolf W. Berg,[1a] and Niels J. Bjerrum[1a]

Received July 31, 1985

Green $KV(SO_4)_2$ crystals were synthesized by dissolution of V_2O_5 in a $KHSO_4$ melt at 450 °C under SO_2(g) atmosphere. Slow cooling of the solution from 450 to 250 °C in 3 weeks gave small crystals that were used for X-ray structure determination and for obtaining oriented-crystal Raman and infrared spectra. The crystal structure, in rhombohedral (trigonal) space group $R\bar{3}$ with $a = b = 4.781$ (1) Å and $c = 23.545$ (5) Å at −130 °C and $Z = 3$, consists of a unique arrangement of tetrahedral SO_4^{2-} linked to octahedrally coordinated vanadium(III). The structure is compared to other closely related $M^IM^{III}(SO_4)_2$ structures. Infrared spectra on powder and on crystals along c could be assigned conclusively. Raman spectra were measured from small oriented single crystals by using different light polarizations. Anomalous polarization and preresonance enhancement of certain Raman bands were observed. Ten Raman-active modes were predicted by group-theoretical analysis whereas the experiments showed the presence of eleven bands. The extra band at ~1560 cm^{-1} was attributed to a d ← d electronic Raman transition, ν_e, $^3E_g \leftarrow {}^3A_g$, of vanadium(III) in the trigonal crystal field.

Introduction

The chemistry of vanadium(V) oxide dissolved in molten $KHSO_4$–$K_2S_2O_7$ mixtures has been thoroughly investigated[2-6] due to the catalytic importance of these melts in the commercial oxidation of SO_2 to SO_3 for the production of sulfuric acid.[7] During the work[6] we unexpectedly discovered the formation of a green precipitate, which proved to be crystals of $KV(SO_4)_2$. Apparently this compound, mentioned previously in the literature,[8-11] seems to have a quite low solubility not only as known in aqueous sulfuric acid solutions but also in $KHSO_4$–$K_2S_2O_7$ melts in equilibrium with a SO_2 atmosphere. The pressure- and temperature-dependent solubility of $KV(SO_4)_2$ is presently under investigation and will be reported elsewhere.[6]

The present work is concerned with the fundamental properties of the $KV(SO_4)_2$ compound. The crystal structure is determined, the selection rules and correlation diagram for the vibrational properties of the crystal are derived, and the Raman and infrared spectra are presented and assigned according to the group-theoretical considerations.

Synthesis of Crystalline $KV(SO_4)_2$

The green compound, $KV(SO_4)_2$ has previously been prepared (i) by concentrating sulfuric acid solutions containing potassium and vanadium,[8,9] (ii) by bubbling SO_2 gas through potassium pyrosulfate–potassium vanadate melts,[10] and (iii) by tempering a finely ground 1:1 solid mixture of K_2SO_4 and $V_2(SO_4)_3$.[11]

The possibility of isolating the salt from $KHSO_4$ melts containing dissolved vanadium oxides under a SO_2 atmosphere was discovered during our spectroscopic investigations,[6] where bright green crystals appeared in the spectroscopic cuvettes.

In order to prepare large single crystals suitable for X-ray structure and spectroscopic investigations, long-term precipitation procedures were followed: $KHSO_4$ and V_2O_5 or V_2O_4 were added to Pyrex ampules (molar fraction X_{KHSO_4} = ca. 0.983) that were sealed off under 0.9 atm of SO_2.

As described previously,[4] the $KHSO_4$ used was from Merck (Suprapure or Pro Analysi) and was dried at 110 °C for 3 days and subsequently stored and handled in a glovebox with dry-nitrogen atmosphere. V_2O_5 and V_2O_4 from Cerac (Pure, 99.9 and 99.5%, in the form of sized nonhygroscopic granules) were used without further purification. The purity of SO_2 was better than 98% by volume. After fusion and equilibration at 450 °C, the melts had formal concentrations of vanadium at ~0.5 mol/L, based on the known density.[3]

The ampules had estimated gas to melt volume ratios sufficiently large to secure an excess of SO_2 even after complete reduction to V(III) of the vanadium present. Bright green solutions were obtained within a few hours. The speed of dissolution seemed much faster for V_2O_5 than for V_2O_4. The latter oxide probably dissolves through a redox process since a gas (possibly SO_2) was evolved from the contact zone between the melt and solid. The melts were gently rocked overnight at 450 °C, in a Kanthal-wire-wound quartz-tube furnace with a water-cooled glass jacket (temperature precision within 5 °C). Then, the temperature was reduced to 425 °C and kept there for 1 week. A yellow-green crystalline precipitate slowly separated out. The temperature was further gradually reduced to 250 °C in steps of 25 °C during a period of 8 weeks. As the temperature decreased, the color of the melts changed gradually from green to blue, ending up as almost clear at 250 °C, indicating that the melts were nearly completely empty of vanadium.

The crystals were finally isolated by cutting the ampules open and gently flushing the solidified content with water, which slowly during several days dissolved the $KHSO_4$ but not the $KV(SO_4)_2$.

The crystals were examined under a polarization microscope, and proper crystals were selected for the investigations.

The chemical analysis[6] of the compound with respect to V and K was in accordance with the formula $KV(SO_4)_2$.

On heating, the bright green color of $KV(SO_4)_2$ faded toward yellow-green, until the compound finally decomposed at ~450 °C.

X-ray Investigations

Powder Diffraction. The X-ray powder diffraction pattern of a sample quoted to be $KV(SO_4)_2$ has been published by Perret,[11] who indexed his pattern in a monoclinic cell with $a = 8.16_4$ Å, $b = 5.14_8$ Å, $c = 7.87_0$ Å, $\beta = 94°\ 20'$, $Z = 2$, $D_{calcd} = 2.836$ g cm^{-3}, and $D_{exptl} = 2.81$ g cm^{-3}, probably closely analogous to the yavapaiite $KFe(SO_4)_2$ structure[12-14] in space group $C2/m$.

(1) (a) Technical University of Denmark. (b) University of Münster. (c) Institute of Chemical Engineering and High Temperature Processes, University of Patras, Gr-26110 Patras, Greece. (d) Visiting Professor at the Technical University of Denmark in 1984.
(2) Hansen, N. H.; Fehrmann, R.; Bjerrum, N. J. *Inorg. Chem.* **1982**, *21*, 744.
(3) Hansen, N. H.; Bjerrum, N. J. *J. Chem. Eng. Data* **1981**, *26*, 13.
(4) Fehrmann, R.; Hansen, N. H.; Bjerrum, N. J. *Inorg. Chem.* **1983**, *22*, 4009.
(5) Fehrmann, R.; Gaune-Escard, M.; Bjerrum, N. J. *Inorg. Chem.*, in press.
(6) Fehrmann, R.; Hansen, N. H.; Bjerrum, N. J.; Philipsen, J.; Pedersen, E., to be submitted for publication.
(7) Sittig, M. "Sulfuric Acid Manufacture and Effluent Control", Chemical Process Review No. 55; Noyes Data Corp.: Park Ridge, NJ, 1971.
(8) Rosenheim, A.; Mong, H. Y. *Z. Anorg. Allg. Chem.* **1925**, *148*, 25.
(9) Sieverts, A.; Müller, E. L. *Z. Anorg. Allg. Chem.* **1928**, *173*, 313.
(10) Frazer, J. H.; Kirkpatrick, W. J. *J. Am. Chem. Soc.* **1940**, *62*, 1659.
(11) Perret, R. *Bull. Soc. Fr. Mineral. Cristallogr.* **1971**, *94*, 84.
(12) Hutton, C. O. *Am. Mineral.* **1959**, *44*, 1105.
(13) Graeber, E. J.; Rosenzweig, A. *Am. Mineral.* **1971**, *56*, 1917.
(14) Anthony, J. W.; McLean, W. J.; Laughon, R. B. *Am. Mineral.* **1972**, *57*, 1546.

0020-1669/86/1325-1571$01.50/0

Table I. Observed and Calculated X-ray Powder Pattern for $KV(SO_4)_2$[a]

h k l	I_{obsd}	$\sin^2\theta_{obsd}$	$\sin^2\theta_{calcd}$[b]
0 0 3	5	0.009 29	0.009 53
1 0 4	10	0.051 21	0.051 60
0 0 9	4	0.085 42	0.085 77
1 0 8	3	0.102 19	0.102 43
1 1 0	6	0.103 91	0.103 98
1 1 3	3	0.113 68	0.113 51
1 0 10	2	0.140 01	0.140 55
1 1 6	5	0.141 54	0.142 21
2 0 4	5	0.154 98	0.155 58
1 0 11	1	0.161 72	0.162 79
2 0 5	1	0.164 53	0.165 11
2 0 8	4	0.205 57	0.206 41
0 0 15	1	0.236 82	0.238 25
1 0 14	1	0.241 00	0.242 21
2 0 10	1	0.244 28	0.244 53
1 1 12	6	0.256 26	0.256 46
2 1 4	6	0.258 93	0.259 56
1 0 16	1	0.305 60	0.305 70
3 0 0	7	0.311 68	0.311 94
1 1 15	4	0.341 34	0.342 20

[a] Virtually unground sample. When the sample was ground, the powder pattern changed, perhaps due to partial decomposition. [b] $\sin^2\theta$ values were calculated from the cell parameters originating from the powder work: $a = b = 4.7771$ (5) Å, $c = 23.669$ (1) Å, $\gamma = 120°$, $\lambda = 1.5404$ Å. A SiO_2 standard was used.

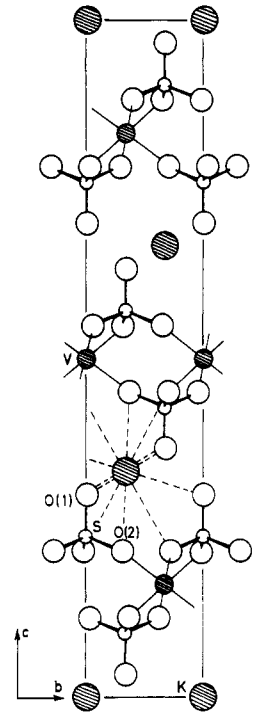

Figure 1. Projection of the unit cell of $KV(SO_4)_2$ parallel to (100).

We obtained the X-ray powder diffraction diagram of our $KV(SO_4)_2$ on a sample of finely ground crystalline hexagons, by using a Guinier camera and monochromated Cu Kα radiation ($\lambda = 1.5418$ Å). When a hexagonal (trigonal) cell with $a = b = 4.790_1$ Å, $c = 23.78_5$ Å, $\gamma = 120°$, $Z = 3$, $D_{calcd} = 2.975$ g cm^{-3}, and $D_{expti} = 2.99$ (2) g cm^{-3} is chosen, the pattern can be indexed as shown in Table I. The diffraction lines of Perret cannot be matched with our recorded lines, and the two samples must be different phases. This conclusion is amplified, noting the difference in density and crystal system, and we believe that he probably prepared another modification of $KV(SO_4)_2$ than we did. The existence of more than one modification among compounds $M^IM^{III}(SO_4)_2$ depending on the method of preparation has previously been noted for the case of $TlV(SO_4)_2$ etc.[15]

Determination of Crystal Structure by Single-Crystal X-ray Diffraction Analysis. Intensity data were collected on a Syntex $P2_1$ single-crystal diffractometer at −130 °C (143 K), using a thin, light green, transparent, hexagonal, platelike crystal as a sample.

The high-precision unit cell dimensions were refined from a number of high-angle reflection coordinates determined on the four-circle diffractometer. No phase transition was observed between +20 and −130 °C, and the single-crystal diffraction results were in accordance with the powder data. The single-crystal data and pertinent details on data collection and refinement of the structure are given in Table II. In Table III the coordinates of the atoms at −130 °C are shown (the thermal

(15) Perret, R.; Couchot, P. *C. R. Seances Acad. Sci., Ser. C* **1972**, *274*, 55.

Table II. Crystal Data, Data Collection, and Refinement of the Structure at −130 °C for $KV(SO_4)_2$[a]

fw	282.17
Laue symmetry	$\bar{3}$
cryst syst	rhombohedral (trigonal)
space group	$R\bar{3}$-C_{3i}^2, S_6^2 (No. 148)
unit cell, hexagonal setting	
a, Å	4.781 (1) [4.782 (1)]
c, Å	23.545 (5) [23.644 (5)]
V, Å^3	466.1 [468.2]
Z	3
systematic extinctions	hkl; $-h + k + l = 3n$
unit cell, rhombohedral setting	
a, Å	8.320 (2) [8.351 (2)]
α, deg	33.40 (2) [33.27 (2)]
V, Å^3	155.4 [156.1]
Z	1
systematic extinctions	none
D_{calcd}, g cm^{-3}	3.015 [3.002]
D_{expti}, g cm^{-3}	[2.99 (2)]
cryst size, mm^3	0.28 × 0.28 × 0.04 (hexagonal plate ∥ (001))
radiation	Mo Kα, $\bar{\lambda} = 0.710\,69$ Å, graphite monochromatized
abs coeff, cm^{-1}	29.9
abs corr	ψ scan
data collcn range	$2° \le \theta \le 27°$
no. of reflcns measd	812 (half sphere)
no. of reflcns after averaging	232, of which 211 had $I \ge 1.96\sigma(I)$
scan mode	2θ–θ
scan speed, deg min^{-1}	4–30, according to intensity
scan range in 2θ, deg	2.0 + $\alpha_{1,2}$ splitting
no. of variables	20
structure solution[b]	from Patterson function in $R\bar{3}$
refinement	full-matrix least squares
weighting scheme	$1/w = \sigma^2\|F_o\| + (0.008\|F_o\|)^2$
$R_1 = \sum\|\|F_o\| - \|F_c\|\|/\sum\|F_o\|$	0.049
$R_2 = [\sum w(\|F_o\| - \|F_c\|)^2/(\sum w\|F_o\|^2)]^{1/2}$	0.042

[a] Values at 20 °C are given in brackets. [b] The computations were done on a Data General Eclipse S/200 computer using modified Syntex EXTL programs and the SHELXTL program system of G. M. Sheldrick.

Table III. Coordinates of the Atoms in the Hexagonal Unit Cell at −130 °C for $KV(SO_4)_2$[a]

	site	*x*	*y*	*z*
K	3a	0	0	0
V	3b	0	0	0.5
S	6c	0	0	0.23858 (7)
O(1)	6c	0	0	0.30035 (21)
O(2)	18f	0.2797 (8)	0.3066 (8)	0.21688 (13)

[a] The temperature factor coefficients are given in the supplementary material.

Table IV. Interatomic Distances (Å) and Bond Angles (deg) with Standard Deviations in Parentheses for $KV(SO_4)_2$

K–O(1)	2.867 (1) (6×)		
K–O(2)	3.275 (1) (6×)		
V–O(2)	1.996 (4) (6×)	O(2)–V–O(2′)	88.5 (2) (6×)
		O(2)–V–O(2″)	91.5 (2) (6×)
S–O(1)	1.455 (5)	O(1)–S–O(2)	110.0 (2) (3×)
S–O(2)	1.496 (5) (3×)	O(2)–S–O(2′)	109.0 (2) (3×)

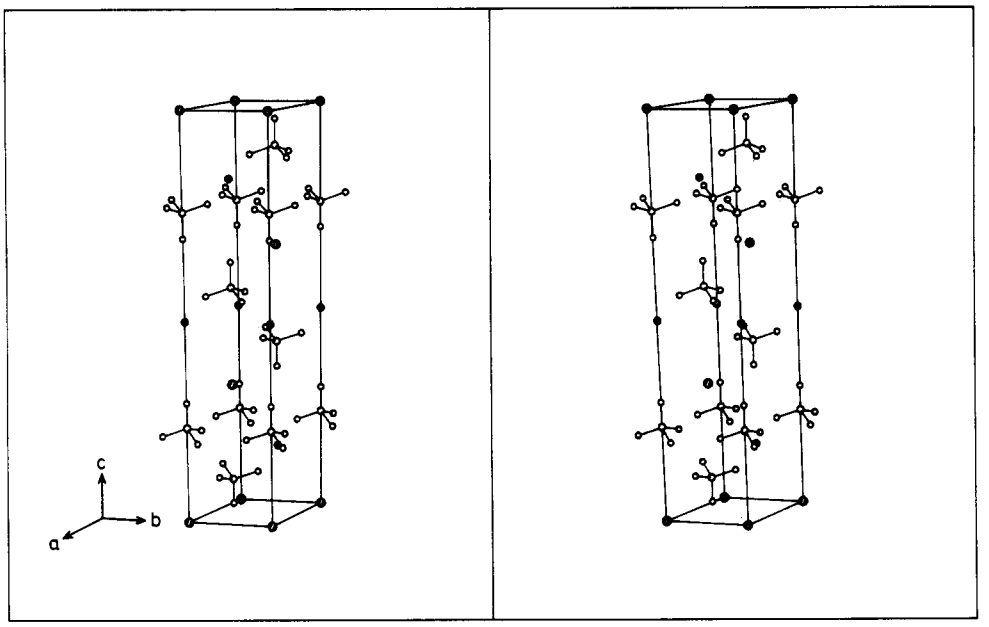

Figure 2. Stereo plot of the unit cell of $KV(SO_4)_2$.

Table V. Structural Features of Double-Sulfate Types

$M^IM^{III}(SO_4)_2$	space group	coordn of M^I	coordn of M^{III}	quotient of ionic radii M^I/M^{III}	refs
$KAl(SO_4)_2$	$P321$	6 + 6	6 (trigonal prismatic)	0.38	1–3
$KFe(SO_4)_2$	$C2/m$	10	6 (octahedral)	0.48	4
$RbTl(SO_4)_2$	$R32$	6 + 6	6 (trigonal prismatic)	0.64	5
$KV(SO_4)_2$	$R\bar{3}$	6 + 6	6 (octahedral)	0.56	this work

parameters are given in the supplementary data). Figures 1 and 2 give a projection and a stereopair of the rhombohedral structure in the hexagonal setting of the unit cell. The important interatomic distances and bond angles of the structure are collected in Table IV. A table of observed and calculated structure factors is available as supplementary material.

Discussion of the Crystal Structure

The crystal structure consists of a unique arrangement of tetrahedral SO_4^{2-} anions linked to octahedrally coordinated vanadium(III) and to K^+ ions in a 6 + 6 oxygen coordination, formed by an elongated trigonal antiprism of O(2) atoms with an equatorial corrugated hexagon of O(1) atoms. As shown in Figure 1, the VO_6 octahedra are corner- or edge-connected to the SO_4^{2-} tetrahedra and form a triple polymeric layer of composition $[V(SO_4)_2^-]_n$ centered at $z = {}^1/_6$, ${}^1/_2$, and ${}^5/_6$. These triple sheets are separated by layers of K^+ ions, also parallel (001), situated at $z = 0$, ${}^1/_3$, and ${}^2/_3$. This layerlike arrangement with the weakest bonds between K^+ and the triple $[V(SO_4)_2^-]_n$ sheets is reflected in the platelike habit of the crystals and their easy cleavage parallel to (001). The VO_6 octahedron is regular within the limits of error whereas the S–O(1) and S–O(2) bond lengths within the SO_4^{2-} ion are significantly different. This may be due to the stronger interaction of the triply coordinated O(2) (besides S: one V is at 1.996 Å and one K^+ is at 3.275 Å) with vanadium as compared to the weaker interaction of the tetrahedrally coordinated O(1) (besides S: three K^+ are at 2.867 Å) with potassium. It is also reflected in the splitting of the degenerate vibrations in the IR and Raman spectra (see below).

The found crystal structure of $KV(SO_4)_2$ is unique: Apparently, there is no other example of this structure type known in the structural chemistry of double sulfates and of other non-sulfate double salts of this stoichiometry as well.

The previously known structure prototypes are (i) the trigonal ($P321$) $KAl(SO_4)_2$ structure of many anhydrous alums,[16–18] including $RbV(SO_4)_2$ and $CsV(SO_4)_2$,[19] (ii) the monoclinic ($C2/m$) $KFe(SO_4)_2$ structure, represented by the mineral yavapaiite,[12–15] including $KV(SO_4)_2$ as prepared by Perret[11] and $NaV(SO_4)_2$ and $AgV(SO_4)_2$,[20] (iii) the rhombohedral ($R32$) $RbTl(SO_4)_2$ type,[15,20,21] including one modification of $TlV(SO_4)_2$,[15,20] and (iv) a set of lanthanoid double sulfates such as $LiEu(SO_4)_2$ and $LiPr(SO_4)_2$,[22] $NaNd(SO_4)_2$ and $NaEr(SO_4)_2$,[23] and $CsLa(SO_4)_2$.[24]

There is a remarkably close relationship between our $KV(SO_4)_2$ structure and the former three types $KAl(SO_4)_2$, $KFe(SO_4)_2$, and $RbTl(SO_4)_2$ (see also ref 21). All four structures contain very similar triple sheets of composition $[M^{III}(SO_4)_2^-]_n$ with M^{III} = Al, Fe, V, or Tl alternating with layers of alkali-metal ions, the thickness of such a cation–anion layer package being around 8 Å. The difference within the members of the structural family consists of a different coordination of the metal centers, especially the M^{III} metals. In Table V some features of the prototype structures are listed. One determining factor for the different structures may be the different absolute size and ratio of the metal atom ionic radii. The relationship between the $RbTl(SO_4)_2$[21] and $KV(SO_4)_2$ structure types is especially close: The shapes of the unit cells are very similar; the change from space group $R32$ to $R\bar{3}$ retains all the atomic positions with the only exception of O(2), thus changing the coordination of M^{III} from trigonal-prismatic thallium(III) to octahedral vanadium(III). To make sure that the $KV(SO_4)_2$ structure is really different from the similar $RbTl(SO_4)_2$ type of Laue symmetry $\bar{3}m$ (instead of $\bar{3}$ in $KV(SO_4)_2$), the deviations from the higher Laue symmetry were

(16) Vegard, L.; Maurstad, A. *Z. Kristallogr., Kristallogeom., Kristallphys., Kristallchem.* **1929**, *69*, 519.
(17) Manoli, J.-M.; Herpin, P.; Pannetier, G. *Bull. Soc. Chim. Fr.* **1970**, 98.
(18) Franke, W.; Henning, G. *Acta Crystallogr.* **1955**, *19*, 870.
(19) Strupler, N. *Bull. Soc. Chim. Fr.* **1970**, 2451.
(20) Perret, R.; Thrierr-Sorel, A.; Couchot, P. *Bull. Soc. Fr. Mineral, Cristallogr.* **1972**, *95*, 521.
(21) Pannetier, G.; Manoli, J.-M.; Herpin, P. *Bull. Soc. Chim. Fr.* **1972**, 485.
(22) Sirotinkin, S. P.; Efremov, V. A.; Kovba, L. M.; Pokrovskii, A. N. *Kristallografiya*, **1977**, *22*, 966; **1978**, *23*, 406.
(23) Sirotinkine, S. P.; Tchijov, S. M.; Pokrovskii, A. N.; Kovba, L. M. *J. Less-Common Met.* **1978**, *58*, 101.
(24) Bukovec, N.; Kaučič, V.; Golič, L. *Acta Crystallogr., Sect B: Struct. Crystallogr. Cryst. Chem.* **1980**, *B36*, 129.

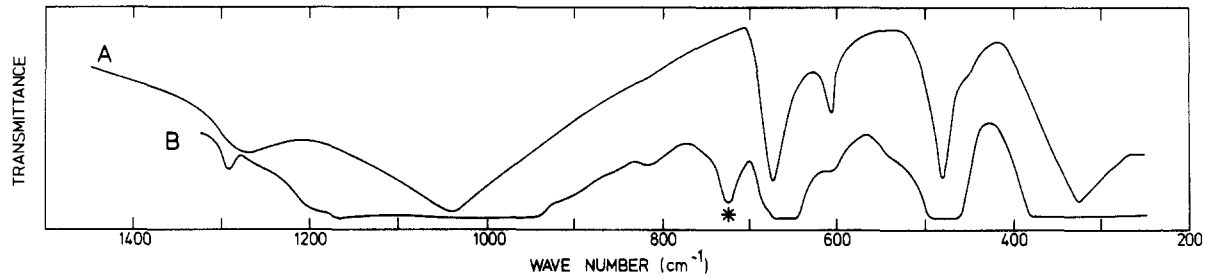

Figure 3. Infrared spectra of $KV(SO_4)_2$ (A) as a powder in pressed KBr disk and (B) as a mosaic of thin crystal plates oriented in paraffin, such that the light travels along the crystallographic c axes. The band at $\sim$730 cm^{-1} with an asterisk is due to paraffin. No IR band was recorded above 1500 cm^{-1}.

Table VI. Analysis of the Selection Rules for $KV(SO_4)_2$, Space Group S_6^2 ($R\bar{3}$, No. 148)[a]

S_6 point group	T_A	T	R	N_i	Raman activity	IR activity
A_g		1	1	3 (ν_1, ν_3, ν_4)	x^2+y^2, z^2	
E_g		1	1	3 (ν_2, ν_3, ν_4)	(x^2-y^2, xy) (xz, yz)	
A_u	1	2	1	3 (ν_1, ν_3, ν_4)		z
E_u	1	2	1	3 (ν_2, ν_3, ν_4)		x, y

[a] The Bravais primitive cell contains one formula with K on Wyckoff site 3a (S_6 symmetry), V on site 3b (S_6 symmetry), S and O(1) on sites 6c (C_3 symmetry), and O(2) on site 18f (C_1 symmetry). T_A = the number of inactive acoustic modes, T = the number of optic branch translatory modes, R = the number of rotatory modes (of SO_4^{2-}), and N_i = the number of internal modes (of SO_4^{2-}).

checked very carefully; so there is no doubt about the lower symmetry of the novel $KV(SO_4)_2$ structure type. It might be worthwhile to check the $R32$ symmetry of the $RbTl(SO_4)_2$ structure type by a set of precise intensity measurements in order to make sure that it is really not identical with the $KV(SO_4)_2$ type.

The structure of $KV(SO_4)_2$ does not show any disorder or other signs of anomalous behavior, which might give a ready explanation for extra Raman bands (see below).

Infrared and Raman Spectra

General Considerations. The standard analysis of the crystal selection rules, based on group-theoretical principles[25-27] in the wave vector $\mathbf{k} = 0$ approximation, is obtained and summarized in Table VI. From this table it appears that a total of 10 Raman-permitted fundamentals (5 A_g + 5 E_g) and 12 IR-permitted fundamentals (6 A_u + 6 E_u) should be spectroscopically observable by letting suitably polarized light interact with powders or oriented crystals (as indicated in the last two columns of Table VI).

A further feature is shown in Table VI. In crystals containing complex ions (here SO_4^{2-}), vibrations are commonly separated into internal modes (N_i, of sulfate) and external modes (rotational (R) and translational (T) lattice modes). The internal vibrations of a regular tetrahedral SO_4^{2-} ion (T_d point group) span the representation

$$\Gamma_{vib} = A_1(\nu_1) + E(\nu_2) + 2\,F_2(\nu_3 + \nu_4)$$

of which all are Raman- and F_2 IR-permitted. Modes labeled ν_1 and ν_3 are stretchings, and ν_2 and ν_4 are bendings.

In $KV(SO_4)_2$, the two SO_4^{2-} ions present in the Bravais unit cell have a total of $2(3 \times 5 - 6) = 18$ internal degrees of vibrational freedom, which should be distributed on the symmetry species and original sulfate modes ν_1–ν_4 as shown in Table VII. The frequencies of the fundamentals of the SO_4^{2-} ion have been well

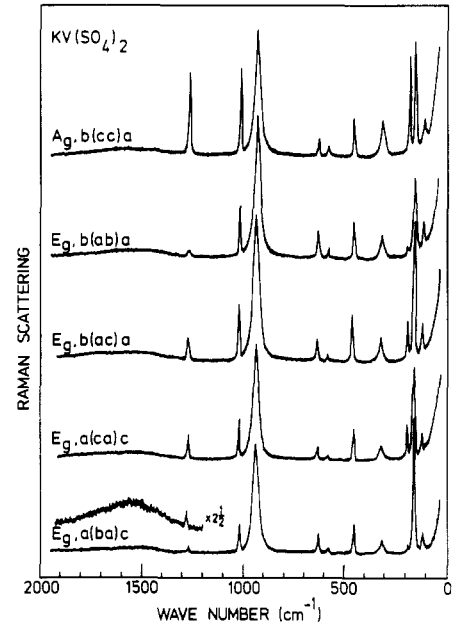

Figure 4. Raman spectra of $KV(SO_4)_2$ at room temperature of an oriented crystal of approximate size 0.1 × 1.0 × 1.0 mm^3 (λ_0 514.5 nm, power $\sim$100 mW, resolution $\sim$2 cm^{-1}).

characterized previously,[28,29] mainly by Raman spectroscopy on aqueous solutions:

$$\nu_1(A_1) \simeq 981\ cm^{-1} \qquad \nu_2(E) \simeq 451\ cm^{-1}$$
$$\nu_3(F_2) \simeq 1104\ cm^{-1} \qquad \nu_4(F_2) \simeq 613\ cm^{-1}$$

The close approach of ions and the lowering of symmetry within the crystal are expected to shift the fundamentals moderately and to split degeneracies, but it should still be possible to identify the stretchings (ν_1 and ν_3) and the bendings (ν_2 and ν_4). Many examples of thorough vibrational analyses of sulfates are described in recent literature, e.g. for Li_2SO_4,[30] Na_2SO_4,[31] K_2SO_4,[32-35] and double sulfates of these,[36,37] and also melts have been carefully studied.[38,39]

(25) See e.g.: Fateley, W. G.; McDevitt, N. T.; Bentley, F. F. *Appl. Spectrosc.* **1971**, *25*, 155.
(26) Adams, D. M. *Coord. Chem. Rev.* **1973**, *10*, 183. Adams, D. M.; Newton, D. C. *Tables for Factor Group and Point Group Analysis*; Beckman-RIIC: Croydon, England, 1970.
(27) Rousseau, D. L.; Bauman, R. P.; Porto, S. P. S. *J. Raman Spectrosc.* **1981**, *10*, 253.
(28) Siebert, H. *Anwendungen der Schwingungsspektroskopie in der Anorganischen Chemie*; Springer-Verlag: Berlin, 1966.
(29) Nakamoto, K. *Infrared and Raman Spectra of Inorganic and Coordination Compounds*; Wiley: New York, 1978.
(30) Frech, R.; Cazzanelli, E. *Solid State Ionics* **1983**, *9&10*, 95.
(31) Montero, S. *Spectrochim. Acta, Part A* **1976**, *32A*, 843.
(32) Montero, S.; Schmölz, R.; Haussühl, S. *J. Raman Spectrosc.* **1974**, *2*, 101.
(33) Meserole, F.; Decius, J. C.; Carlson, R. E. *Spectrochim. Acta, Part A* **1974**, *30A*, 2179.
(34) Brooker, M. H. *Appl. Spectrosc.* **1975**, *29*, 528.
(35) Wu, G.-J.; Frech, R. *J. Chem. Phys.* **1976**, *64*, 4897.
(36) Raghunatha Chary, B.; Bhat, H. L.; Chandrasekhar, P.; Narayanan, P. S. *Curr. Sci.* **1984**, *53*, 980.
(37) Frech, R.; Teeters, D. *J. Phys. Chem.* **1984**, *88*, 417.
(38) Smith, D. H.; Begun, G. M.; Child, W. C., Jr. *J. Chem. Soc., Faraday Trans. 2* **1981**, *77*, 1399.

Table VII. Correlation Diagram for SO_4^{2-} Internal Vibrations[a]

two isolated ions of T_d symmetry	two isolated ions on sites of C_3 symmetry	two ions in Bravais unit cell of S_6^2 symmetry
$2A_1$ (ν_1(str))	6A (ν_1(str), ν_3(str), ν_4(bend))	$3A_g$ (ν_1(str), ν_3(str), ν_4(bend))
2E (ν_2(bend))		$3E_g$ (ν_2(bend), ν_3(str), ν_4(bend))
$4F_2$ (ν_3(str), ν_4(bend))	6E (ν_2(bend), ν_3(str), ν_4(bend))	$3A_u$ (ν_1(str), ν_3(str), ν_4(bend))
		$3E_u$ (ν_2(bend), ν_3(str), ν_4(bend))

[a] The site symmetry is C_3, and the unit cell symmetry is S_6, with the 3 and $\bar{3}$ axes fixed to the crystallographic c axes.

Table VIII. Infrared and Raman Bands (cm^{-1}) of $KV(SO_4)_2$ and Their Assignments[a]

IR powder (Figure 3A)	IR cryst (Figure 3B)	Raman cryst (Figure 4)	tentative assignt	SO_4^{2-} vib freq[b]
		~1560 w(vbr)	$\nu_e(^3E_g \leftarrow {}^3A_g)$[c]	
1260 s	~1290 w		$\nu_3(A_u)$	
		1288 m	$\nu_3(A_g)$	
1030 vs	~1050 vs (vbr)		$\nu_3(E_u)$	1105 (ν_3)
		1038 m	$\nu_3(E_g)$	
		958 s (br)	$\nu_1(A_g)$	983 (ν_1)
662 vs	~670 vs (br)		$\nu_4(E_u)$	
		652 w	$\nu_4(E_g)$	611 (ν_4)
		600 w	$\nu_4(A_g)$	
595 s	~600 w		$\nu_4(A_u)$	
		474 m	$\nu_2(E_g)$	
466 vs	~470 vs (br)		$\nu_2(E_u)$	450 (ν_2)
		335 w (br)	$\nu_L(A_g)$[d]	
314 s	~300 vs (br)		$\nu_L(E_u)$	
		205 m	$\nu_L(A_g)$	
		174 m	$\nu_L(E_g)$	
		130 m	$\nu_L(E_g)$	

[a] Intensity codes: w = weak; m = medium; s = strong; v = very; (br) = broad. [b] Aqueous solution; ref 29, p 142. [c] ν_e = electronic mode. [d] ν_L = external lattice mode.

Infrared Spectra. IR spectra of $KV(SO_4)_2$ at room temperature (see Figure 3) were obtained (a) on finely ground powders in pressed KBr disks and (b) on mosaic arrays of thin crystal plates (typically of 0.05-mm thickness, held together by a layer of paraffin, mp ca. 50 °C, and mounted across a 1 × 5 mm hole in a copper plate). The predominant natural (001) sheetlike habit of the crystals made the orientation easy because the sixfold axes (along c perpendicular to the sheets) automatically became the light direction, and any crystallite rotation around this direction is unnecessary under symmetry $R\bar{3}$. The IR spectra were recorded on Beckman IR-20 and Perkin-Elmer 437 spectrometers in double-beam mode against (a) an empty KBr disk and (b) a thin sheet of paraffin and a mechanical attenuator. The IR bands can easily and unambiguously be assigned according to the selection rules as shown in Table VIII. The bands that significantly lost intensity when going from powder to crystal were assigned to A_u modes because such bands should be inactive for the light traveling along c. The A_u component of ν_1 is probably very weak, and two lattice modes, expected below 300 cm^{-1}, are unobserved.

Infrared spectra of a large number of hexagonal ($P321$) $M^IM^{III}(SO_4)_2$ salts in KBr disks have previously been recorded and assigned.[40,41] These IR spectra were largely identical with our spectrum in Figure 3A. Interestingly, the monoclinic $KFe(SO_4)_2$ and apparently also Perret's monoclinic $KV(SO_4)_2$ showed more extensive splitting, especially of ν_4, in accordance with what should be expected in a low-symmetry crystal.

Raman Spectra. Raman spectra (see examples in Figure 4) were measured at room temperature on three oriented single crystals and on a polycrystalline sample (not shown). Similar spectra were obtained at 77 K on samples in sealed ampules immersed in liquid N_2. For excitation, krypton and argon ion laser lines were used. With the krypton 647.1- and 676.4-nm lines, no spectra were obtained due to strong light absorption and decomposition of the sample. The argon 514.5-, and 488.0-, and 457.9-nm lines resulted in essentially identical spectra, but small changes in the relative intensities were observed. The scattered light was collected at an angle of 90° and sent through a 90° image rotator and a polarization scrambler, the entrance slit being vertical and the scattering plane horizontal. A JEOL JRS-400D 0.4-m double monochromator and a cooled S-20 photomultiplier with photon counting were applied and calibrated to ±1 cm^{-1} with a neon discharge lamp. In Figure 4, the polarization of the exciting and scattered light was varied by using a $\lambda/2$ plate and a Polaroid-sheet polarizer as indicated in the standard labeling $x(yz)q$. (Expressed in crystallographic directions, $x(yz)q$ exactly describes the experiment and hence the selection rules; x = excitation direction, y = excitation polarization direction, z = collection polarization direction, and q = collection direction.)

Ten Raman bands are expected (Tables VI and VII) in the crystal spectra (5 A_g and 5 E_g). The centrosymmetry excludes the bands from being seen in both IR and Raman spectra (gerade–ungerade classification). From Figure 4 and Table VIII it can be seen that 11 instead of 10 bands are present in the Raman spectra. Furthermore, the spectra (Figure 4) show polarization abnormalities, mainly with respect to the five A_g modes. Thus, it is expected that, relative to the $b(cc)a$ configuration, five bands should diminish in intensity in other configurations (or even disappear). This happens, to some extent, only for the two bands at 1288 and 205 cm^{-1}, which are assigned to A_g symmetry. For the remaining bands the polarization data cannot be used to distinguish their symmetries.

It should be noted that the orientation of the single crystals was definitely correct due to the easily recognized direction of the c axis, which was perpendicular to the flat side of the crystal. However, it may be argued that the small size and flatness of the crystal (and perhaps other causes like optical anisotropy) may invalidate to some extent the theoretical separations among transitions belonging to A_g and E_g symmetries and make bands to "leak" quite strongly in all configurations. In our view, as presented below, these anomalous polarizations can be attributed to possible interactions between the vibrational and electronic states in the crystal.

From a series of Raman and infrared measurements of sulfate crystals and sulfate solutions,[28-41] it is evident that the $\nu_1(A_g)$ mode of $KV(SO_4)_2$ ought to be intense and be in the frequency range 900–1000 cm^{-1}. Thus, the strong band at 958 cm^{-1} is assigned to A_g. Other bands below 1300 cm^{-1} are tentatively assigned to symmetries as given in Table VIII.

The broad and weak band at 1560 cm^{-1} is attributed to an electronic Raman transition of the V^{3+} ion. A characteristic feature of the electronic Raman bands is that they are generally much broader than vibrational bands, even at very low temperatures.[42,43] The possibility that the 1560-cm^{-1} band could be due to smeared-out overtones/combinations from throughout the Brillouin zone was ruled out because the band did not lose in intensity by cooling to ~70 K.

(39) Child, W. C., Jr.; Begun, G. M.; Smith, D. H. *J. Chem. Soc., Faraday Trans. 2* **1981**, *77*, 2237.
(40) Couchot, P.; Mercier, R.; Bernard, J. *Bull. Soc. Chim. Fr.* **1970**, 3433.
(41) Couchot, P.; Nguyen Minh Hoang, F.; Perret, R. *Bull. Soc. Chim. Fr.* **1971**, 360.
(42) Koningstein, J. A. *Mol. Spectrosc.* **1976**, *4*, 196. Koningstein, J. A. *Vib. Spectra Struct.* **1981**, *9*, 115.
(43) Clark, R. J. H.; Dines, T. J. *Adv. Infrared Raman Spectrosc.* **1982**, *9*, 282.

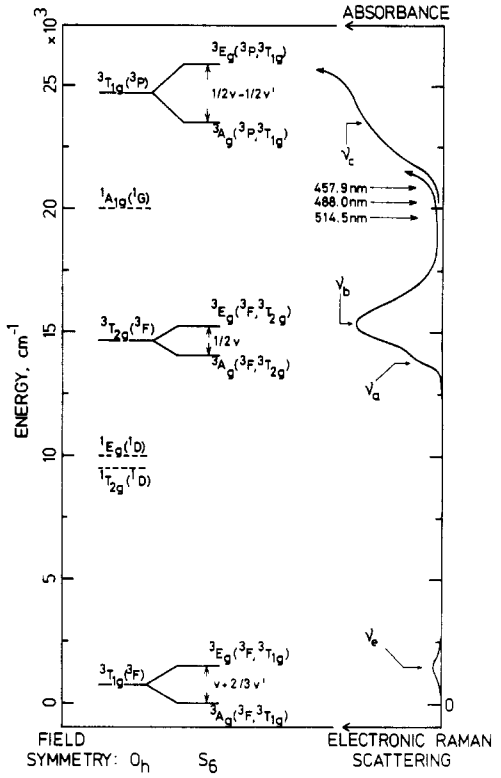

Figure 5. Energy states of V^{3+} with Dq = 1600 cm^{-1} in octahedral O_h field. Broken lines indicate spin-forbidden states associated with spin-forbidden transitions from the ground state. The splitting of triplet states in trigonal S_6 field is shown in the middle. To the right, the absorption[6] and electronic Raman spectra are reproduced in arbitrary intensity units.

The ground electronic state of V^{3+} (d^2) in an octahedral crystal field is $^3T_{1g}(^3F)$, which in the trigonal S_6 field splits into an upper ^3E_g and a ground ^3A_g state.[44,45] Similar splittings occur in the two excited triplet states $^3T_{2g}(^3F)$ and $^3T_{1g}(^3P)$. In Figure 5, we have estimated the electronic states of V^{3+} in octahedral oxide fields using a theoretical energy diagram[45] with the Dq parameter $\approx$1600 cm^{-1}. In the same figure the absorption spectrum of solid $KV(SO_4)_2$ measured by Fehrmann et al.[6] is also presented. The observed bands in the visible region are attributed to V^{3+} transitions in the S_6 crystal field

$$^3A_g(^3F, ^3T_{2g}) \leftarrow {}^3A_g(^3F, ^1T_{1g}) \qquad \nu_a \approx 13\,900 \text{ cm}^{-1}$$

$$^3E_g(^3F, ^3T_{2g}) \leftarrow {}^3A_g(^3F, ^1T_{1g}) \qquad \nu_b \approx 15\,300 \text{ cm}^{-1}$$

and the shoulder band in the near-UV region is assigned to the split component, ^3A_g, of the second triplet exited state $^3T_{1g}(^3F)$

$$^3A_g(^3P, ^3T_{1g}) \leftarrow {}^3A_g(^3F, ^3T_{1g}) \qquad \nu_c \approx 23\,500 \text{ cm}^{-1}$$

The separation of the $^3A_g(^3T_{2g})$ and $^3E_g(^3T_{2g})$ states is $\Delta\nu = \nu_b - \nu_a \approx 1400$ cm^{-1}, which according to ligand field calculations[44,45] is smaller than the separation of $^3E_g(^3T_{1g})$ and $^3A_g(^3T_{1g})$ in the ground state. In other words, for the V^{3+} ion in the $KV(SO_4)_2$ crystal the first electronic Raman transition is likely to occur in a region near and above 1400 cm^{-1}. The broad Raman band at $\sim$1560 cm^{-1} is in this expected range and is thus assigned to the $^3E_g(^3T_{1g}) \leftarrow {}^3A_g(^3T_{1g})$ electronic transition. Such a transition is permitted according to the electronic Raman selection rules since the direct product $A_g \otimes E_g$ includes the representation E_g, which belongs to the Raman polarizability tensor components.[42,43]

On the basis of crystal field model calculations, the splitting of the octahedral states in trigonal fields of intermediate strength can be calculated in terms of the two parameters v and v'.[44-46]

For the triplet states in Figure 5 the splittings are

$$\Delta[^3T_{1g}(^3F)] = v + \tfrac{2}{3}v'$$

$$\Delta[^3T_{2g}(^3F)] = \tfrac{1}{2}v$$

$$\Delta[^3T_{1g}(^3P)] = \tfrac{1}{2}(v - v')$$

The values of the first two splittings, measured from the spectra, are $\sim$1560 and $\sim$1400 cm^{-1}, respectively, and thus v = 2800 cm^{-1} and v' = $-$1860 cm^{-1}. From the third difference the energy of the upper $^3E_g(^3P, ^3T_{1g})$ state can be estimated to $\sim$26 800 cm^{-1}, based on ν_c = 23 500 cm^{-1}.

The green to blue laser lines used to excite the Raman spectra overlap with the tail of the Laporte-allowed UV absorption bands $^3A_g(^3P, ^3T_{1g})$ and $^3E_g(^3P, ^3T_{1g})$, and it is likely that the electronic and vibrational Raman intensities exhibited preresonance enhancement.[43] Measurements of the band intensities relative to the intensity of the 474-cm^{-1} $E_g(\nu_2)$ Raman band were conducted with the 514.5-, 488.0-, and 457.9-nm Ar^+ lines. The reference band at 474 cm^{-1} was chosen because, as seen in Figure 4, it remains constant for all spectral configurations. The relative intensities were measured after taking into account the instrument function (efficiency of grating and photomultiplier at different wavelengths) in the configurations $c(aa)b$ and $c(bc)b$. As the color changed from green (514.5 nm) to blue (457.9 nm), the relative intensities of the Raman bands exhibited the following variations:

(i) They increased for all high-frequency vibrational bands (region 950–1300 cm^{-1}). Thus, the intensities of $\nu_1(A_g)$, $\nu_3(E_g)$, and $\nu_3(A_g)$ increased by $\sim$60, $\sim$30, and $\sim$100%, respectively.

(ii) They increased by $\sim$200% for the electronic band ν_e.

(iii) All bands arising from the ν_2 and ν_4 bending modes remained unchanged (region 340–652 cm^{-1}).

(iv) Bands due to the external lattice modes (region below 300 cm^{-1}) decreased slightly ($\sim$20%).

It should be emphasized that these variations are measured relative to the 474-cm^{-1} band and that intensities of spectra obtained with different exitation lines cannot be compared since there is no common reference band available (for example a solvent or a matrix band).

It is apparent from the above observations that the Raman spectra of $KV(SO_4)_2$ exhibit electronic and vibrational transitions that are in preresonance with the $^3A_g(^3P, ^3T_{1g})$ and $^3E_g(^3P, ^3T_{1g})$ electronic states of the V^{3+} ion in the UV region. Furthermore, the ground electronic state is spin-degenerate, and as has been pointed out previously,[43,47,48] this results in spin–orbit degenerate state functions that in turn mix with totally symmetric vibrational states, leading to "anomalous" depolarization effects. To us, the observed spectra (Figure 4) are examples of these effects, thus breaking the selection rules predicted by the standard group-theoretical analysis. As far as we know, this is the first time an electronic Raman effect of V^{3+} has been observed.[49]

Conclusion

Examination of the compound $KV(SO_4)_2$ has been performed: It has a unique structure in space group $R\bar{3}$ that allows for the interpretation of the IR spectrum and, by incorporating the electronic Raman effect and "anomalous" depolarization effects, also the Raman spectrum.

Acknowledgment. This investigation has been supported by the "Stimulation Actions" program of the European Economic Community (EEC Contract No. STI-011-J-C(CD)) and by the Reinholdt W. Jorck og Hustrus Fond (J. No. 46/1982). Erik Pedersen and Ole Sonnich Mortensen of Copenhagen and Odense Universities are thanked for experimental assistance and helpful

(44) Hush, N. S.; Hobbs, R. J. M. *Prog. Inorg. Chem.* **1968**, *10*, 259.
(45) Ferguson, J. *Prog. Inorg. Chem.* **1970**, *12*, 159.
(46) Macfarlane, R. M. *J. Chem. Phys.* **1964**, *40*, 373.
(47) Hamaguchi, H.; Harada, I.; Shimanouchi, T. *Chem. Phys. Lett.* **1975**, *32*, 103. Hamaguchi, H. *J. Chem. Phys.* **1978**, *69*, 569.
(48) Clark, R. J.; Turtle, P. C. *J. Chem. Soc., Faraday Trans. 2* **1976**, *72*, 1885.
(49) After completion of this work, the electronic Raman effect was observed also in $CsV(SO_4)_2 \cdot 12H_2O$ and $NH_4V(SO_4)_2 \cdot 12H_2O$ with $\nu_e \cong$ 1940 cm^{-1}; see: Best, S. P.; Clark, R. J. H. *Chem. Phys. Lett.* **1985**, *122*, 401.

comments. Also, we thank the Fonds der Chemischen Industrie for financial support.

Registry No. $KV(SO_4)_2$, 14520-79-7; $KHSO_4$, 7646-93-7; V_2O_5, 1314-62-1; V_2O_4, 12036-21-4; SO_2, 7446-09-5.

Supplementary Material Available: A table of observed and calculated structure factors and a table (Table IX) of coordinates of the atoms in the unit cell and temperature factor coefficients for $KV(SO_4)_2$ at −130 °C (3 pages). Ordering information is given on any current masthead page.

Contribution No. 3795 from the Central Research & Development Department, Experimental Station, E. I. du Pont de Nemours & Company, Wilmington, Delaware 19898

Heteropolyanions of the Types $M_3(W_9PO_{34})_2^{12-}$ and $MM'M''(W_9PO_{34})_2^{12-}$: Novel Coordination of Nitrate and Nitrite

W. H. Knoth,*† P. J. Domaille, and R. L. Harlow

Received August 21, 1985

Reaction of A-$W_9PO_{34}^{9-}$ with divalent Mn, Fe, Ni, Cu, Zn, and Pd gives anions of the formula $M_3(W_9PO_{34})_2^{12-}$, similar to $Co_3(W_9PO_{34})_2^{12-}$ we previously reported; reaction with Ce(IV) gives $(OCe)_3(W_9PO_{34})_2{\cdot}2H_2O^{12-}$. A crystal structure of the latter clearly shows the geometry of the anion although most of the K^+, H_3O^+, and H_2O species that surround the anion are disordered: $K_9(H_3O)_3[(Ce_3O_3{\cdot}2H_2O)(W_9PO_{34})_2]{\cdot}26(?)H_2O$; $W_{18}Ce_3K_9P_2O_{102}H_{65}$; monoclinic, $C2/m$; at −100 °C, a = 33.219 (4) Å, b = 15.903 (1) Å, c = 17.385 (2) Å, β = 98.41°, Z = 4. Several nitrate and nitrite complexes are also described; the crystal structure of $Cu_3(W_9PO_{34})_2{\cdot}NO_3^{13-}$, which has a nitrate group reversibly coordinated within the central skeletal cavity, is reported: $K_{11}\{[Cu_3(NO_3)](W_9PO_{34})_2\}(H_3O)_2{\cdot}28(?)H_2O$; $W_{18}Cu_3K_{11}P_2O_{101}NH_{62}$; monoclinic, $P2_1/m$; at −100 °C, a = 12.224 (3) Å, b = 33.502 (8) Å, c = 12.346 (4) Å, β = 118.29 (1)°, Z = 2. Other nitrate and nitrite complexes are also described. Further reactions of the $M_3(W_9PO_{34})_2^{12-}$ anions lead to related species with dissimilar belt metals. Examples include $Zn_2(O_2W)(W_9PO_{34})_2^{12-}$, $Cu_2Co(W_9PO_{34})_2{\cdot}NO_3^{13-}$, $NiCu(O_2W)(W_9PO_{34})_2^{12-}$, and $CoFe(O_2W)(W_9PO_{34})_2^{12-}$.

Introduction

We have pursued our earlier discovery[1] that unthermolyzed $Na_8HW_9PO_{34}$[2] has an A-type structure and reacts with cobalt(II) to form $(H_2OCo)_3(A\text{-}W_9PO_{34})_2^{12-}$, whereas thermolyzed (150 °C) $Na_8HW_9PO_{34}$ has a B-type structure and is known[3-5] to react with cobalt(II) to form $(H_2O)_2Co_4(B,\alpha\text{-}W_9PO_{34})_2^{10-}$. This paper reports a number of analogues of $(H_2OCo)_3(A\text{-}W_9PO_{34})_2^{12-}$, including some with two or three dissimilar metals between the W_9P moieties, and some chemistry of these anions, including novel coordination of nitrate and nitrite ions. Crystal structures of two anions are included.

Results and Discussion

A. $(OCe)_3(A,\alpha\text{-}W_9PO_{34})_2^{12-}$. Reaction of ceric ammonium sulfate with $W_9PO_{34}^{9-}$ gives a yellow anion that can be precipitated as a potassium salt. This initial product displays four ^{31}P NMR lines (−6.32, −6.97, −7.64, and −8.33 ppm at pH 4.7) of variable intensities, establishing that it is a mixture. After the mixture is refluxed in water for 1 h, the spectrum changes to that of a single species (^{31}P NMR: one line, −7.57 ppm at pH 5.2). The ^{183}W NMR spectrum of this single species consists of two lines, at −151.9 and −161.1 ppm in a 1:2 ratio. The latter line is very broad but sharpens considerably on lowering the pH to 3.1 (HCl). The sharper line displays tungsten–tungsten coupling ($^2J_{W\text{-}O\text{-}W}$ = 14.3 Hz). These data, together with analysis of several salts, suggest a structure consisting of two A-type $W_9PO_{34}^{9-}$ units connected by a belt of three cerium atoms.

A crystal structure determination on $Ce_3(W_9P)_2$ reveals that it is really $(OCe)_3(W_9PO_{34})_2{\cdot}2H_2O^{12-}$ (Figure 1) in the solid state. The belt contains three oxygen atoms alternating with the three cerium atoms; two of the latter also have external water ligands. The presence of the bridging oxygen atoms in the final product offers an explanation for the ^{31}P NMR observations. The initial product may be a mixture of $[(HO)_2Ce]_3(W_9P)_2$ and its successive condensation products $(HO)_2Ce(HOCe)_2O(W_9P)_2$, $(HOCe)_2O_2Ce(W_9P)_2$, and $(OCe)_3(W_9P)_2$ with complete condensation to the last occurring during the subsequent reflux period.

The crystal structure of $(OCe)_3(W_9P)_2$ confirms not only that it contains A-W_9P groups but that these are A,α, not A,β. The same is true of a copper complex discussed later. These structures make it quite likely that the starting material, unthermolyzed $Na_8HW_9PO_{34}$, also has an A,α-W_9P group, not an A,β-W_9P group.

B. Other $M_3(A,\alpha\text{-}W_9PO_{34})_2^{12-}$ Anions. The reactions of A,α-$W_9PO_{34}^{9-}$ with divalent manganese, iron, cobalt, nickel, copper, zinc, and palladium in water proceed rapidly to give anions of the type $L_nM_3(A,\alpha\text{-}W_9PO_{34})_2^{x-}$. The ligands L may be nitrate or nitrite as discussed later or water as in the case of $(H_2OCo)_3(W_9PO_{34})_2^{12-}$, which we reported previously.[1] We have not established the presence or absence of aquo ligands in the other species described here. Potassium salts of all these anions have quite similar infrared spectra (see Figure 9 in ref 1 for the spectrum of the cobalt complex) from 1200 to 600 cm^{-1} and are presumably isostructural. The skeletal structure postulated earlier[1] for the cobalt complex $Co_3(A\text{-}W_9PO_{34})_2$ is consistent with a crystal structure done on $Cu_3(W_9PO_{34})_2{\cdot}NO_3^{13-}$ (see Figure 2 and discussion later), which provides the additional information that the W_9P groups are α.

Potassium salts of the $Co_3(W_9P)_2$ and $Zn_3(W_9P)_2$ anions are converted to the corresponding $(H_2O)_2M_4(B,\alpha\text{-}W_9P)_2$ salts in boiling water, as shown by elemental and infrared analyses and by the ^{183}W NMR spectrum[5] of the zinc complex. $Cu_3(W_9P)_2$ is changed in boiling water to an anion whose potassium salt analyses for $K_{10}(H_2O)_2Cu_4(W_9PO_{34})_2$. However, the infrared spectrum of this product is grossly different from that of the other $M_4(W_9P)_2$ salts and it cannot have an identical structure. The P–O region exhibits four bands (1137, 1100, 1072, 1043 cm^{-1}) in the P–O region compared to the maximum of three for a nondegenerate PO_4 spectrum and the degenerate or nearly degenerate (20-cm^{-1} splitting at most) P–O bands we observe for the other $M_4(W_9P)_2$ salts. The established $M_4(W_9P)_2$ structure[4] calls for the metal M to assume octahedral coordination; this is difficult for copper(II) because of the Jahn–Teller effect.

The manganese, iron, and nickel $M_3(W_9P)_2$ complexes are also unstable in boiling water; infrared analysis suggests the major

† Present address: Box 6, Mendenhall, PA 19357.

(1) Knoth, W. H.; Domaille, P. J.; Farlee, R. D. *Organometallics* **1985**, *4*, 62–68.
(2) Massart, R.; Contant, R.; Fruchart, J. M.; Ciabrini, J. P.; Fournier, M. *Inorg. Chem.* **1977**, *16*, 2916–2921.
(3) Tourné, C.; Revel, A.; Tourné, G.; Vendrell, M. *C. R. Seances Acad. Sci., Ser. C* **1973**, *277*, 643–645.
(4) Weakley, T. J.; Evans, H. T., Jr.; Showell, J. S.; Tourné, G. F.; Tourné, C. M. *J. Chem. Soc., Chem. Commun.* **1973**, 139.
(5) Finke, R. G.; Droege, M.; Hutchinson, J. R.; Gansow, O. *J. Am. Chem. Soc.* **1981**, *103*, 1587–1589.

0020-1669/86/1325-1577$01.50/0